Depletion-induced colloidal crystals at a wall characterised by small-angle X-ray diffraction

X. Xian,[a] A.V. Petukhov,[a*] M.M.E. Snel,[b] I.P. Dolbnya,[c] D.G.A.L. Aarts,[a] G.J. Vroege[a] and H.N.W. Lekkerkerker[a]

[a]van `t Hoff laboratory for physical and colloidal chemistry, Debye Institute, Utrecht University, 3508 TB Utrecht, The Netherlands, [b]Physical Chemistry of Interfaces, Utrecht University, 3508 TB Utrecht, The Netherlands, and [c]DUBBLE CRG/ESRF, the Netherlands Organisation for Scientific Research, ESRF BP220, F-38043, Grenoble Cedex, France. E-mail: a.v.petukhov@chem.uu.nl

Silica photonic colloidal crystals on a flat glass substrate have been grown using the depletion attraction induced by nonadsorbing polymers. The dried samples have been characterised with high-resolution synchrotron small-angle X-ray diffraction and their surface topography has been studied by atomic force microscopy. The presence of long-range ordered crystals with a thickness as large as 90 planes is demonstrated. However, on some places the films are polycrystalline and contain disordered regions.

Keywords: small-angle X-ray diffraction; wall crystals; depletion-interaction-induced growth, colloids

1. Introduction

The past decade saw an ever-increasing importance of photonic crystals, in which the band-structure concepts of solid-state physics are applied to microwave, radio and optical waves. For example, photonic crystals are a powerful platform for guiding optical light through air, which reduces losses; they could be useful components in fibre-optics communications and high-speed optical computing (Joannopolous, 2001). To achieve all this, the idea is to design periodic structures that would do for electromagnetic waves what a semiconductor crystal does for electron waves. Large-scale fabrication of photonic structures is a challenging problem. Conventional semiconductor nanofabrication techniques (Krauss *et al*., 1996), which have been adapted to make photonic structures, are costly and difficult to extend to larger scale. Yet a potentially simpler and cheaper way to create large-scale three-dimensional periodic structures is through self-assembly of colloidal spheres.

Colloidal crystals, which are supported on a substrate, are easy to be integrated into larger circuits and, thus, are of importance for future applications. One of the techniques to assemble colloidal spheres on a flat substrate, the so-called controlled drying technique (Denkov *et al*., 1992; Jiang *et al*., 1999; Vlasov *et al*., 2001; Velikov *et al.*, 2002*a*), exploits capillary forces of the solvent-air interface as the meniscus is swept along a vertical substrate due to solvent evaporation. Here we use a different technique: a depletion-induced fluid-solid phase transition at a wall (de Hoog *et al*., 2001; Kaplan *et al*., 1994; Bringer *et al.*, 1999; Dinsmore *et al.*, 1997; Kose & Hachisu, 1976). This transition is caused by the addition of free, nonadsorbing polymers to a colloidal dispersion. A phase separation occurs due to the so-called depletion interaction between the colloids. The region around the colloidal particle (grey shadowed in Fig. 1) is the depletion zone, from which the mass centres of the polymers are excluded. When colloidal particles approach each other sufficiently closely, their depletion zones overlap, which causes an imbalance in osmotic pressure exerted by the polymers. This imbalance induces an effective attraction between the colloidal particles.

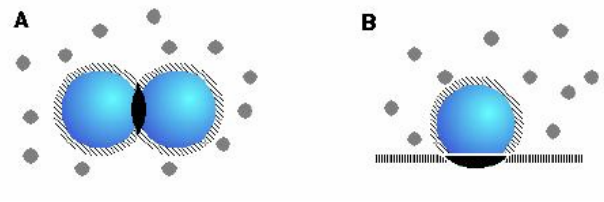

Figure 1

Overlap volume of depletion zones between two spherical particles (A) and between a sphere and a flat wall (B). Larger and smaller spheres denote hard-sphere colloidal particles and penetrable polymer random coils, respectively. The shadowed region around colloids is the depletion zone and dark areas mark their overlap.

When the polymer concentration is high enough, the attraction will be sufficiently strong to separate the colloid-polymer suspension into a colloid-rich phase and a colloid-poor one. As a flat hard wall also has a depletion zone, overlap of colloidal particles with this zone (which at contact is about twice the overlap volume between two particles, implicating that the effective attraction is twice as large too) results in colloid-rich layers in contact with the wall (see Fig. 1(*B*).

Investigation of the structural properties of photonic materials is an important step in their development. A significant amount of information on the local structure can be gained with microscopy techniques, such as electron, atomic force (AFM) and confocal scanning laser microscopy (Gasser *et al*., 2001). These techniques, however, are unable to address the crystalline order on a large scale. Moreover, while confocal microscopy allows three-dimensional imaging within a restricted region, only the two-dimensional surface topography can be addressed in electron and scanning probe techniques. Diffraction techniques can directly probe the reciprocal q space parameters, averaged over macroscopic scales, which are relevant for photonic applications. Light scattering (Dux & Versmold, 1997) significantly suffers from multiple scattering and is able to probe only low diffraction orders. A much wider range of diffraction wave vectors can be successfully probed with small angle neutron (Dux *et al*., 1996) and X-ray (Vos *et al.*, 1997; Petukhov *et al*., 2002) diffraction. Moreover, X-rays from modern synchrotron sources allow achieving a resolution of the order of 10^{-6}th part of the X-ray wavevector, which is sufficient to study the long-range-order on (sub)millimetre distances (Petukhov *et al*., 2002).

In this work, small angle X-ray diffraction (SAXD) was used to characterise the wall crystals after drying. The diffraction patterns were taken at different places in the sample and different sample orientations. The reciprocal lattice reflections are found to be very sharp as evidenced by detecting the pattern modifications induced by small sample tilts. Quantitatively this result indicates the presence of interplanar positional order over ~ 90 layers, which is presumably limited by the thickness of the wall crystal. To have a view of the topography of the surface of the crystal, AFM tapping mode was used.

2. Experimental

The wall crystals were made by putting microscope glass cover slips vertically into a suspension of sterically stabilized, spherical silica colloids with non-adsorbing polymers in cyclohexane as the solvent according to the method of de Hoog *et al*. (2001). After a few days crystals were formed at the wall.

The silica colloids were provided by Verhaegh *et al.* (1998). These colloids have a silica-core with a diameter of 42 nm, which was first covered with a silica layer containing a fluorescent dye and then grown with a pure silica coating to a final diameter of 230 nm. To avoid van der Waals attraction between silica spheres, the so-called steric stabilisation is applied. For this the particles are coated with a monolayer of 1-octadecanol (stearyl alcohol, Merck). These silica spheres behave as hard spheres in solvent cyclohexane and are shown to form long-range-ordered (sub)millimetre crystals (Petukhov *et al.*, 2002).

A suspension of these colloids and non-absorbing poly(dimethylsiloxane) polymers with a molecular weight of 97 kg/mol, a density of 0.976 g/ml and a radius of gyration of 13 nm in the solvent cyclohexane was prepared. The volume fraction of the polymer, which shows how much space is filled by random polymer coils, was in the range from $\phi_p = 0.15$ to 0.249. The volume fraction of colloid in the suspension was $\phi_c = 0.06$ to 0.07. These volume fractions were chosen, because the suspension lies around the phase boundary, which means that the polymer concentration is sufficiently high to induce phase separation (de Hoog *et al.*, 2001).

The glass slips of Chance Propper Ltd (about 0.125 mm thick) were used as a support. They were cleaned by keeping them in chromic acid for 24 h, rinsed with demineralised water and dried in air. The next step was to put them in a melt of 1-octadecanol at 195°C for about 4 h. Holders made of copper wires were used in order to move the glass slips easily in and out of the hot melt. Finally, the glass slips were removed and the unreacted stearyl alcohol was cleaned with chloroform. The hydrophobic surface of the glass slips was tested by a water droplet on the surface, which was non-wetting, indicating that the surface of the glass plate has become a "steric layer". So the colloids, which have also been coated with stearyl alcohol, will interact with the glass plate solely via the hard-wall potential. After preparing the glass slips and the suspension, the glass slips were placed in little bottles with the concentrations as described above. Cyclohexane is extremely volatile. To prevent too fast evaporation of the solvent, the bottles were put in a rectangular glass-box with a (nearly) saturated cyclohexane atmosphere. Inside the box a large bowl with cyclohexane was placed. It was observed that the sedimentation of the silica particles was faster than the drying of the suspension. So the crystals did not grow by capillary forces as in a controlled drying method (Denkov *et al.*, 1992; Jiang *et al.*, 1999; Vlasov *et al.*, 2001; Velikov *et al.*, 2002*a*). After three days the suspension was totally dried and the glass slips were removed from the bottles. Visual inspection of the glass slides revealed that in the top part, the glass slip was almost transparent. In the middle part, the glass slip showed green Bragg reflections since the interplanar distance in close-packed crystals equals half the wavelength of green light in the crystal. This is the part where good crystals were expected. The very bottom part of the glass slide was in the (dried) sediment area. It is covered by a thick layer of colloid and no clear Bragg reflections were seen.

The synchrotron SAXD experiments were performed at the BM26 "DUBBLE" beam line of the European synchrotron radiation facility (E.S.R.F.) in Grenoble, France. The samples were mounted on a goniometer allowing sample rotation around the vertical and horizontal axes normal to the beam. In addition, the goniometer was placed on two translation stages in order to probe various places on the glass slides. The goniometer and the translation stages were controlled by a computer outside the experimental hutch. The quasi-monochromatic X-ray beam had a photon energy of 14.7 keV (wavelength $\lambda = 0.084$ nm), bandwidth $\Delta\lambda/\lambda = 2 \times 10^{-4}$ and a beam size of 100×100 microns^2 at the sample. Diffraction was detected at 8 metres distance from the sample by a 13×13 cm^2 two-dimensional gas-filled detector. The direct beam was absorbed by a 5×5 mm^2 lead beam-stop hanging at the end of a vacuum fly-path tube, which is used to minimise unwanted scattering of X-rays by air between the sample and the detector. The maximum diffraction angle at the edge of the detector and the minimum angle at the edge of the beam stop were about $2\theta_{max} = 7$ and $2\theta_{min} = 0.2$ mrad, respectively. These allow us to access a range of the diffraction wavevectors of $0.016 < q < 0.5$ nm^{-1} ($q = 4\pi\sin\theta/\lambda$). After the X-ray diffraction experiment some of the glass slips were also characterised with tapping mode AFM (Nanoscope III multimode, Digital Instruments). Silicon cantilevers (126 μm long) with a resonance frequency between 290-366 KHZ were used.

3. Results

Fig. 2(*a*) represents a typical diffraction pattern measured in the upper part of the glass slip, on which the crystals were grown at a volume fraction of $\phi_p = 0.249$ and $\phi_c = 0.053$. The pattern is isotropic and is mostly dominated by the form factor, as evidenced in panel (*b*), where the radially-averaged intensity profile is shown. For comparison, the intra-particle scattering function (the form factor), which was measured in a capillary containing a dilute suspension of the same colloidal particles, is also presented. Only at the smallest wavevectors in the vicinity of the edge of the beam stop, one can see an effect of the structure factor. We note that our finite resolution (see also a discussion below) does not allow us to resolve the true depth of the minima of the form factor of our particles. In general, if the intrumental resolution function was known, one could de-smear the experimental data to better resolve the depth of the minima (Glatter & Gruber, 1993).

The AFM picture (Fig. 3) reveals that the upper part of the glass slip here is covered by little islands of colloids grouped together. The height cross-section (panel C of Fig. 3) reveals that the islands are only one monolayer of colloids high on the upper part of the glass slip. Thus, the diffraction in Fig. 2 is not developed into sharp rings (typical for polycrystalline samples) as the islands have too small sizes.

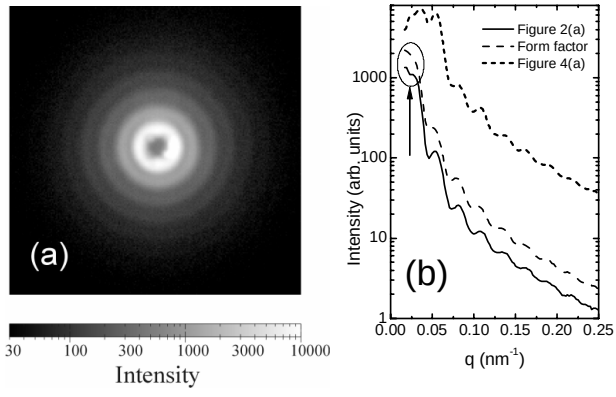

Figure 2

(*a*): SAXD pattern measured in the upper part of the glass slip. (*b*): Averaged radial profile of the pattern shown in panel (a) (solid line). The form factor measured in a capillary containing a dilute suspension of the particles (long dash) is shown for comparison. The arrow points to the small-q region, where one can see an effect of the structure factor. The short-dashed line presents the radial profile of the scattered intensity in Fig.4(*a*).

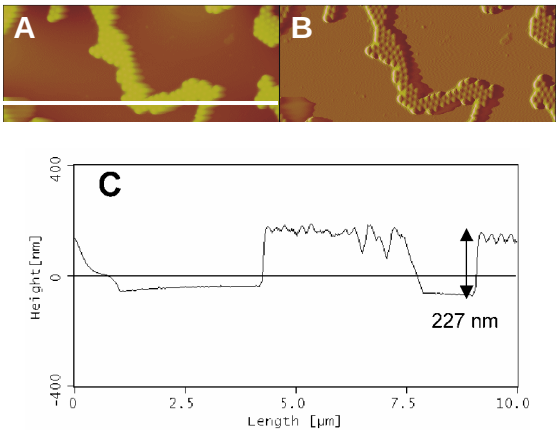

Figure 3

AFM picture obtained in the upper part of the sample. In panel A the height image is shown and in panel B the corresponding amplitude image reveals more detail. Panel C displays the height profile along the white line in (A). Image size is 4.3 x 10 µm. The vertical scale is 1000 nm (A) and 1 V (B)

By translating the sample the SAXD patterns were measured at various positions. It was found that much larger crystals could be found in the lower parts of the glass slip, just above the sediment. Fig. 4(*a*) shows an example of such a diffraction pattern, which is dominated by diffraction from a single crystal. This crystal was grown at a volume fraction of $\phi_p = 0.2$ and $\phi_c = 0.06$. The average radial profile of the scattered intensity is displayed in Fig. 2(*b*) by a short-dashed line. Many high-order reflections can be easily seen in Fig. 4(*a*). The white arrow points to one of the six missing reflections of the same class, which clearly indicates that a close-packed structure is formed. These reflections are of the 422 class of face-centred cubic (fcc) and the 300 class of hexagonal close packed (hcp) crystals and their diffraction wavevector is $q = 4\pi\sqrt{3}/a_{NN} = 21.77/a_{NN}$, where a_{NN} denotes the average nearest-neighbour distance. As illustrated in panel (*b*), this value of q is very close to the third zero of the form factor of a uniform sphere at $q = 21.81/a_0$, where a_0 denotes the sphere diameter. The diffraction pattern of Fig. 4(*a*) thus suggests that $a_{NN} \approx a_0$ within a couple of percent accuracy (at $a_{NN} = 1.02\ a_0$ the form factor of the missing reflections becomes comparable to the form factor of the higher-order reflections visible in Fig. 4(*a*). We also note that the missing reflections indicate that the form factor possesses much deeper minima than the apparently shallow minima shown in Fig. 2(*b*), which are strongly smeared out by the finite detector resolution.

The hexagonal spots of the reciprocal space reveal the regular crystalline arrangement of silica spheres in real space, which form hexagonal layers parallel to the substrate surface. Yet an additional background can be seen, which may be caused by some amorphous areas within the irradiated part of the sample. In the lateral direction the crystal was about 100 µm large, as determined from modification of the diffraction pattern by small sample translations. Such a small crystal size did not allow us to perform crystal rotations within a wide range of angles, which would be needed to study the stacking order between the hexagonal planes (Dux *et al.*, 1996; Vos *et al.*, 1997; Petukhov *et al.*, 2002). However, it was large enough to enable small tilts (of the order of a degree) of the glass slip without losing the crystal out of sight.

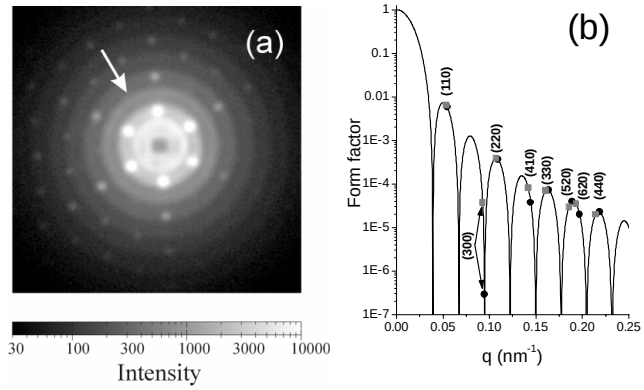

Figure 4

(*a*): SAXD pattern obtained in the middle part of the glass slip. The white arrow points to one of the six missing reflections, which falls into the minimum of the form factor, thus indicating the close-packed arrangement of the micro-spheres. (*b*): Theoretical form factor of a single sphere (solid line). Symbols display values of the form factor for the reflections seen in panel (*a*) for $a_{NN} = a_0$ (dark circles) and $a_{NN} = 1.02\ a_0$ (grey squares). The reflections are denoted using the hcp notation.

For photonic applications the order parameters of colloidal crystals should be of a crucial importance. However, they are very rarely addressed in the literature. In a so-called *perfect* three-dimensional crystal the positions of the 'atoms' (in this case - the colloidal micro-spheres) are correlated throughout the whole crystal. In reality, however, most crystals are *imperfect* (Guinier, 1994). Although they might look ordered locally, various defects and strain fields could easily destroy order on a larger scale. Moreover, the colloidal spheres are never identical to each other but have slightly different sizes, which may also affect the long-range order. Photonic crystals created by the controlled drying technique usually consist of many small orientationally-correlated but positionally-independent domains separated by cracks created during crystal drying (Velikov, 2002*b*). Clearly, these defects can significantly deteriorate the photonic properties of colloidal crystals, for example, by creating a strong scattering background within the photonic gap.

The spatial extent of the positional order can be determined by diffraction techniques from the width δq of the reciprocal lattice reflections. For colloidal crystals the challenge of X-ray diffraction stems from the fact that the sub-micron "atoms" are more than three orders of magnitude larger than the wavelength λ (in the present experiment $a_0 = 2700\lambda$). For crystals possessing positional order over distances Λ as large as 100 lattice periods, the width δq of the diffraction peaks is more than five orders of magnitude smaller than the X-ray wavevector $k_0 = 2\pi/\lambda$. To resolve such a tiny width, one needs to fulfil conditions of coherent interference of diffracted waves over distances much larger than $\Lambda \sim 20$ µm, corresponding to $\sim 2.5 \times 10^5\ \lambda$. This requirement is difficult to meet, even with high-quality synchrotron X-ray radiation. It is the limited *transverse* coherent length together with the finite detector resolution, which determine the apparent width of the reflections in Fig. 4 (full width half maximum here is about 0.01 nm^{-1}). However, in the *longitudinal* direction (along the beam) the condition of coherent interference of the diffracted waves can be more easily fulfilled on much longer distances (Petukhov *et al.*, 2002) in a small-angle X-ray diffraction experiment. Measurements of the rocking curve of a single colloidal crystal then allow achieving a resolution down to $10^{-6}k_0$ (Petukhov *et al.*, 2002), which is sufficient to characterise the intrinsic width of the reflections of a single crystal.

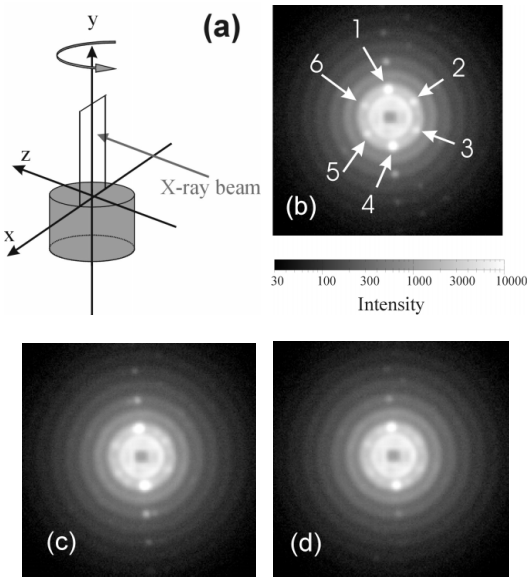

Figure 5

(*a*) Sketch of the sample rotation around the vertical axis and measured diffraction patterns for angles of rotation (relative to the sample orientation in Fig. 4) of (b) -0.5, (c) -1 and (d) 1.5 degrees. Integrated intensities of the six low-order reflections, which are marked in panel A with 1 through 6, are used in evaluation of the width of the reciprocal lattice reflections.

Fig. 5 illustrates the modification of the diffraction pattern upon sample rotation around the vertical axis. A sample tilt by as small as one degree is seen to produce a significant change of the pattern. The six lowest-order spots in the first ring (these correspond to 220-class reflections of fcc crystals and 110-class reflections of hcp structures) were analysed in detail. Reflections 1 and 4 (see the notation scheme introduced in Fig. 5(*a*) do not undergo any significant changes of intensity upon sample tilting since they are closest to the vertical axis of rotation. On the other hand, one can see a drastic reduction of the intensities of the other four spots since here the diffraction vector possesses a nonvanishing component k_z along the crystal axis, normal to the hexagonal planes (which is the ⟨111⟩ axis of fcc or ⟨001⟩ of hcp). The integrated intensities of all six low-order spots were evaluated from the diffraction patterns shown in Figs. 4 and 5 as their FWHM (full width half maximum) times the peak intensity minus the background. Only negligible changes are found for spots 1 and 4. In Fig. 6 the results for the integrated intensity of the other four reflections are plotted against the normalised *z*-component of the diffraction wave vector mismatch $K_z = k_z/b_z$, where $b_z = 2\pi/d_z = 0.033$ nm^{-1} is the basis vector along *z* with d_z being the interplanar spacing in the close-packed structure. Since the crystal was only slightly tilted ($|K_z| \leq 0.03$), the change of the form factor for the reflections in Figs. 4 and 5 is negligible.

The data of Fig. 6 allow us to find the *true* width of the reciprocal lattice reflections. Assuming that the crystal is perfect and consists of *N* positionally-order layers, the structure factor is given by (Guinier, 1994)

$$S(K_z) = \frac{1}{N}\left(\frac{\mathrm{Sin}(N\pi K_z)}{\mathrm{Sin}(\pi K_z)}\right)^2. \qquad (1)$$

The best fit of this structure factor profile to the data (shown in Fig. 6) is obtained with $N = 90$. One has to bear in mind that our data do not allow a very precise evaluation of *N*. However, it certainly falls between $N = 70$ and $N = 120$, as illustrated in the figure. Thus, the *true intrinsic* full width half maximum of the crystal reflections is about 3×10^{-4} nm^{-1}, very much smaller than the apparent width of 0.01 nm^{-1} of the reflections on the detector (Figs. 4 and 5), which is just instrument-limited.

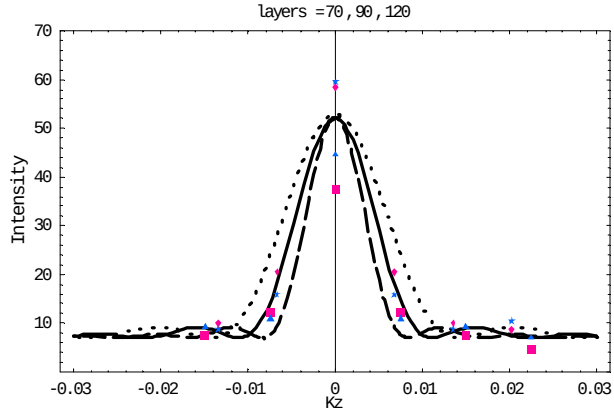

Figure 6

Intensity profiles for the spots 2 (squares), 3 (diamonds), 5 (triangles) and 6 (stars) as a function of the normalised wavevector mismatch K_z. The best fit to the data (shown by the solid line) to Eq.(1) gives $N = 90$. For comparison, curves with $N = 70$ and $N = 120$ are also presented by dashed lines.

The AFM-pictures (see Fig. 7) show that in the bottom part, the colloid population is rather dense. A local crystalline order is visible, which however does not seem to be extended on a large scale. As the AFM tapping mode only reveals the surface topography, nothing can be concluded from this picture about the crystalline order beneath the surface. The relatively strong background (the rings) of the SAXD-pictures in Figs. 4 and 5 could be associated to some randomised amorphous regions, for example, near the surface.

4. Conclusion and outlook

To summarise, in the present work colloidal crystals are grown on a flat substrate, which acts as a carrier. In contrast to the controlled drying technique (Denkov *et al.*, 1992; Jiang *et al.*, 1999; Vlasov *et al.*, 2001, Velikov *et al.*, 2002*a*, Velikov *et al.*, 2002*b*), which exploits capillary forces to assemble colloidal spheres on a flat substrate, we have used depletion attraction forces. The deposition technique is simple and relatively fast. Structure analysis is performed *ex-situ* on dried samples, which have also experienced strong capillary forces. The latter might have introduced an effect on the crystal structure. Synchrotron small-angle X-ray diffraction and atomic force microscopy revealed various types of sample morphology and structure, from a submonolayer deposition of hexagonally-ordered small clusters to a deposition of a thick layer of silica microspheres. In the latter, high-quality long-range ordered crystals as thick as 90 layers can be found. We believe that our results provide a first demonstration of the positional order on such a long distance for colloidal crystals on a flat substrate. However, the SAXD pattern and AFM surface morphology scans reveal the presence of disordered areas as well.

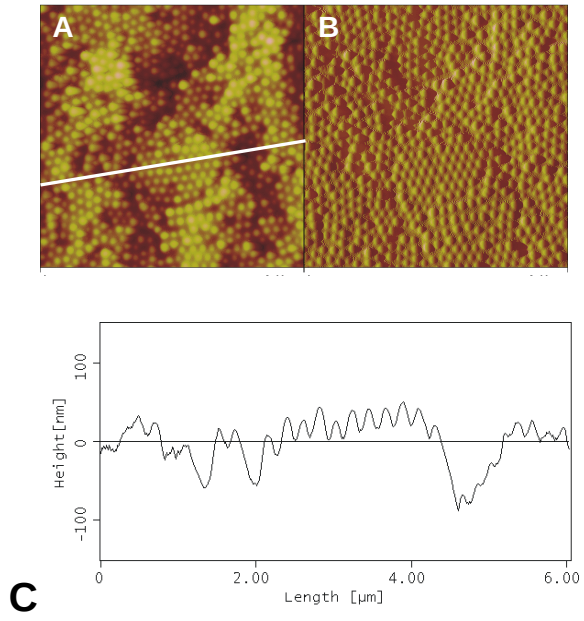

Figure 7

AFM images obtained in the middle part of the glass slip. In panel A the height image is shown and in B the corresponding amplitude image. Panel C displays the height profile along the line indicated in A. The image size is 6 x 6 μm. The vertical scale is 300 nm (A) and 1 Volt (B).

We are currently working on adjustments of the depletion-assisted growth technique to further improve the quality of the wall crystals. We have developed a technique of depletion-induced growth of crystals on the inner walls of a flat glass capillary, which enables us to perform *in-situ* time-resolved investigation of the crystallisation process. Moreover, a combined effect of depletion and capillary forces will be studied *in-situ* and *ex-situ* by varying the polymer concentration and the evaporation rate in a search for the optimal growth conditions.

The authors would like to thank Els de Hoog, Alfons van Blaaderen and Jan van der Eerden for useful discussions. We are grateful to the Netherlands Organisation for the Advancement of Reasearch (NWO) for providing us with the possibility of performing measurements at DUBBLE.

References

Bringer, A., Eisenriegler, E., Schlesener, F. & Hanke, A. (1999). *Eur. Phys. J. B* **11**, 101-119.
de Hoog, E.H.A., de Jong-van Steensel, L.I., Snel, M.M.E., van der Eerden, J.P.J.M. & Lekkerkerker, H.N.W. (2001). *Langmuir* **17**, 5486-5490.
Denkov, N.D.,Velev, O.D., Kralchevsky, P.A., Ivanov, I.B., Yoshimura, H. & Nagayama, K. (1992). *Langmuir* **8**, 3183-3190.
Dinsmore, A.D.,Warren, P.B., Poon, W.C.K., Yodh, A.G. (1997). *Europhys. Lett.* **40**, 337-342.
Dux, C. & Versmold, H. (1997). *Phys. Rev. Let.* **78**, 1811-1814.
Dux, C., Versmold, H., Reus, V., Zemb, T. & Lindner, P. (1996). *J. Chem. Phys.* **104**, 6369-6374.
Gasser, U., Weeks, E.R., Schofield, A., Pusey, P.N. & Weitz, D.A. (2001). *Science* **292**, 258-262.
Glatter, O. & Gruber, K. (1993). *J. Appl. Cryst.* **26**, 512-518.
Guinier, A. (1994). *X-ray Diffraction in Crystals, Imperfect Crystals and Amorphous Bodies.* Dover Publications.
Jiang, D., Bertone, J.F., Hwang, K.S. & Colvin, V.L. (1999). *Chem. Mater.* **11,** 2132-2140.
Joannopoulos, J.D. (2001). *Nature* **414**, 257-258.
Kaplan, P.D., Rouke, J.L., Yodh, A.G. & Pine, D.J. (1994). *Phys. Rev. Lett.* **72**, 582-585.
Kose, A.,Hachisu, S. (1976). *J. Colloid Interface Sci*. **55**, 487-498.
Krauss, T.F., De La Rue, R.M. & Brand, S. (1996). *Nature* **383**, 699-702.
Petukhov, A.V., Aarts, D.G.A.L., Dolbnya, I.P., de Hoog, E.H.A., Kassapidou, K., Vroege, G.J., Bras, W. & Lekkerkerker, H.N.W. (2002). *Phys. Rev. Lett.* **88**, 208301.
Velikov, K.P., Christova, C.G., Dullens, R.P.A. & van Blaaderen**,** A. (2002a). *Science* **296**, 106-109.
Velikov, K.P., Moroz, A. & van Blaaderen**,** A. (2002b). *Appl. Phys. Lett*. **80**, 49-51.
Verhaegh, N.A.M., Asnaghi D., Lekkerkerker, H.N.W. (1998). *Physica* A **264**, 64-74.
Vlasov, Y.A., Xiang-Zheng, B., Sturm, J.C. & Norris, D.J. (2001). *Nature* **414**, 289-293.
Vos, W.L., Megens, M., van Kats, C.M. & Boesecke, P. (1997). *Langmuir* **13**, 6004-6008.

Received 29 August 2002 • Accepted 3 March 2003